

Density functional studies of actinide (III) motexafins (An-Motex²⁺, An = Ac, Cm, Lr). Structure, stability and comparison with lanthanide (III) motexafins

Xiaoyan Cao^{a,b*}, Quansong Li^c, Anna Moritz^a, Zhizhong Xie^c,
Michael Dolg^{a*}, Xuebo Chen^c, Weihai Fang^{c*}

a Institut für Theoretische Chemie, Universität zu Köln, D-50939, Germany

b Biochemistry Department, Zhongshan University, Guangzhou, 510275, P.R. China

c Chemistry Department, Beijing Normal University, Beijing, 100875, P.R. China

* x.cao@uni-koeln.de, m.dolg@uni-koeln.de phone: (00)49-(0)221-470-6894 fax: (00)49-(0)221-470-6896

Fangwh@bnu.edu.cn phone: (00)86-10-58805382 fax: (00)86-10-58802075

25.04.2006

Abstract

Newly developed relativistic energy-consistent 5f-in-core actinide pseudopotentials and corresponding (7s6p5d1f)/[5s4p3d1f] basis sets in the segmented contraction scheme, combined with density functional theory methods, have been used to study the molecular structure and chemical properties of selected actinide(III) motexafins (An-Motex²⁺, An=Ac, Cm, Lr). Structure and stability are discussed and a comparison to the lanthanide(III) motexafins (Ln-Motex²⁺ Ln=La, Gd, Lu) is made. The actinide element is found to reside above the mean N₅ motexafin plane and the larger the cation, the greater the observed out-of-plane displacement. It is concluded that the actinium(III), curium(III), and lawrencium(III) cations are tightly bound to the macrocyclic skeleton, yielding stable structures. However, the calculated metal-ligand gas phase binding energy for An-Motex²⁺ is about 1-2 eV lower than that of Ln-Motex²⁺, implying a lower stability of An-Motex²⁺ compared to Ln-Motex²⁺. Results including solvent effects imply that Ac-Motex²⁺ is the most stable complex in aqueous solution and should be the best candidate for experimentalists to get stable actinide(III) motexafin complexes.

keywords: Actinide(III) motexafin, lanthanide(III) motexafin, density functional theory, molecular structure, pseudopotentials

Introduction

In 1988 a novel expanded porphyrin, texaphyrin, was firstly reported by J.L. Sessler's group in the form of its Cd(II) complex¹. Since then great progress has been made in terms of understanding and exploiting this new class of ligands². Texaphyrins are tripyrrolic, pentaaza macrocycles that have a strong, but "expanded" resemblance to the porphyrins and other naturally occurring tetrapyrrolic prosthetic groups^{3,4}. In contrast to porphyrins, the texaphyrins contain five, rather than four, coordinating nitrogen atoms within their central core, which is roughly 20% larger than that of the porphyrins. Therefore texaphyrins have an ability to form stable 1:1 complexes with a range of larger metal cations (figure 1). In 1993 lanthanide ions were firstly reported by Sessler and coworkers to form stable 1:1 complexes with this type of ligand (lanthanide(III) texaphyrins, Ln-Tex²⁺)⁵. Later, a substitution of the O(CH₂)₃OH side chains of texaphyrins by O(CH₂CH₂O)₃CH₃ yielded motexafins (figure 1), a more stable macrocycle which has been widely used since then. The lanthanide(III) texaphyrins have been found to play an important role in such diverse and potentially beneficial areas as X-ray radiation therapy (XRT), photodynamic therapy (PDT) for oncology, photoangioplasty (PA), and the light-based treatment of age-related macular degeneration (AMD)². They are also able to function as tumor-selective magnetic resonance imaging (MRI) detectable radiation enhancers⁶. Several of these systems, notably motexafin gadolinium (Gd-Tex, XCYTRIN®) and motexafin lutetium (Lu-Tex, LUTRIN®), cf. figure 1b, are attractive candidates for a range of medically relevant applications and are at present being evaluated in advanced clinical trials^{7,8}.

The above exciting achievements in the field of lanthanide(III) texaphyrins have encouraged experimentalists to think about complexes with heavier f-element

homologues and their possible technical usage.⁹ However, in contrast to lanthanides all isotopes of the actinide elements are radioactive, and some of them are relevant for the development of nuclear weapons as well as the production of electricity from nuclear energy. In both cases the radioactive nuclear waste management risks must be addressed sooner or later ¹⁰ and actinide(III) texaphyrins might lead to new approaches in waste remediation. Because of technical limitations associated to working with these highly radioactive species, actinide(III) texaphyrins still remain to be tested experimentally.⁹ Unfortunately, experimentally all attempts in the Sessler group of to synthesize stable actinide(III) texaphyrins have been unsuccessful so far and theoretical investigations of the reasons were encouraged.

From the theoretical point of view the challenge of quantum chemical investigations on systems containing actinide elements arises not from the radioactivity of actinide elements, but from the significant contributions of relativity as well as electron correlation.¹¹ Among the approaches developed in relativistic quantum chemistry the method of ab initio pseudopotentials (PPs) is among the most successful ones.¹² The explicit quantum chemical treatment is restricted to the valence electron system and relativistic effects are implicitly accounted for by a proper adjustment of free parameters in the valence model Hamiltonian. Whereas the first aspect leads to a reduction of the computational effort, the second allows the inclusion of scalar relativistic contributions in a non-relativistic framework. For f-elements several energy-consistent pseudopotentials (PPs) with different core definitions, i.e., 4f-in-core PPs ¹³ as well as 4f-in-valence PPs ¹⁴ ¹⁵ for lanthanides and 5f-in-valence PPs ^{16,17} for actinides, were published by one of the present authors and have been used successfully in various applications by many

researchers . However, due to the well-known stronger involvement of actinide 5f orbitals in chemical bonding the development of 5f-in-core actinide PPs was not attempted so far.

In 2004 we published our studies on the molecular structure and chemical/physical properties of selected lanthanide(III) texaphyrins (Ln-Tex²⁺) using density functional theory applying the B3LYP hybrid functional (DFT/B3LYP) combined with scalar-relativistic energy-consistent 4f-in-core lanthanide pseudopotentials.¹⁸ Good agreement between theoretical and experimental results was obtained. In this paper a similar method, i.e., DFT/B3LYP in connection with new scalar-relativistic energy-consistent 5f-in-core actinide pseudopotentials¹⁹, is applied for actinide(III) motexafins (An-Motex²⁺, An=Ac, Cm, Lr). Furthermore the solvent effects, which were neglected in previous studies on Ln-Tex²⁺, are taken into account by using the COSMO (Conductor-like Screening Model) approach in TURBOMOLE ²⁰. Corresponding calculations have also been carried out for the lighter f-element homologues Ln-Motex²⁺ (Ln = La, Gd, Lu) to enable a 1:1 comparison between the lanthanide and actinide series. We will mainly focus on the structures, stabilities, charge distributions and electron affinities of the molecules considered here. Trends in the actinide series and a comparison with those in the lanthanide series will be attempted by exploiting a near-linear behavior of several properties within each series.

Method

The method of relativistic energy-consistent ab initio pseudopotentials (PPs) is described in detail elsewhere ^{13, 14, 21} and will be outlined here only briefly. The valence-only model Hamiltonian for a system with n valence electrons and N nuclei with charges Q is given as

$$H_v = -\frac{1}{2} \sum_i^n \Delta_i + \sum_{i<j}^n \frac{1}{r_{ij}} + V_{av} + \sum_{I<J}^N \frac{Q_I Q_J}{r_{IJ}}$$

Here i and j are electron indices and I , J are nuclear indices. In the usual approximation the spin-orbit averaged molecular PP V_{av} is simply a superposition of atom-centered PPs

$$V_{av} = \sum_I^N V_{av}^I$$

V_{av}^I denotes a spin-orbit averaged relativistic PP in semilocal form for a core with charge Q_I

$$V_{av}^I = -\sum_i^n \frac{Q_I}{r_{iI}} + \sum_i^n \sum_{l,k} A_{lk}^I \exp(-a_{lk}^I r_{iI}^2) P_l^I$$

P_l^I is the projection operator onto the Hilbert subspace of angular momentum l with respect to center I . The free parameters A_{lk}^I and a_{lk}^I are adjusted to reproduce the valence total energies of a multitude of low-lying electronic states of the neutral atom I and its ions²². Newly developed large-core PPs for actinides modeling the 5fⁿ core (n=0-14 for Ac-Lr) have been used, i.e., the 1s-5f shells were included in the PP core, while all other shells with main quantum number larger than 5 were treated explicitly. 11 valence electrons were included in the calculations for Ac, Cm, Lr corresponding to a trivalent situation, i.e., 0, 7 and 14 electrons are assumed to occupy the 5f shell and are attributed to the PP core for Ac, Cm and Lr, respectively. The 8 electrons of the semi-core 6s and 6p shells as well as the 3 electrons occupying the 6d, 7s and 7p valence shells are taken into account explicitly. The reference data used to determine V_{av} have been taken from relativistic all-electron (AE) calculations using the so-called Wood-Boring

(WB) scalar-relativistic Hartree-Fock (HF) approach. Both AE WB as well as PP calculations have been performed with an atomic finite-difference HF scheme in order to avoid basis set effects in the determination of the PP parameters.

Firstly the s-, p-, d-PP of An (An = Ac, Cm, Lr) were adjusted by choosing the following reference configurations with fixed 5f-occupations ($5f^0$ Ac, $5f^7$ Cm, $5f^{14}$ Lr): An $6d^1 7s^2$, $6d^2 7s^1$, $7s^2 7p^1$, $7s^1 7p^2$, $6d^1 7s^1 7p^1$, $An^+ 6d^2$, $6d^1 7s^1$, $6d^1 7p^1$, $7s^1 7p^1$, $7s^2$, $An^{2+} 6d^1$, $7s^1$, $7p^1$, and An^{3+} , Secondly the reference configurations, $Ac^{10+} 5f^1$, $6f^1$, $7f^1$, $8f^1$, $Cm^{10+} 5f^8$, $5f^7 6f^1$, $5f^7 7f^1$, $5f^7 8f^1$, $Lr^{10+} 5f^{14} 6f^1$, $5f^{14} 7f^1$, $5f^{14} 8f^1$, were chosen for adjusting the f-PP of Ac, Cm, and Lr, respectively. The errors in the total valence energies of finite-difference HF calculations were smaller than 0.004 Hartree, and in energy differences with respect to the ground state less than 0.1 eV.

The (7s6p5d1f)/[5s4p3d1f] ANO Gaussian valence basis sets were generated in the following way. First, (7s6p5d) sets of exponents were energy-optimized in HF calculations for the $6d^1 7s^2$ configuration. Second, the contraction coefficients were obtained from atomic natural orbitals of state-averaged complete active space multi-configuration self-consistent field calculations (CASSCF) with subsequent multi-reference configuration interaction calculations (MRCI). The state-averaging was necessary in order to avoid symmetry-breaking at the orbital level since the applied program MOLPRO is limited to the D_{2h} point group and subgroups. All orbitals were optimized at the CASSCF level, but only the fractionally occupied subshells were treated as active. In the subsequent MRCI calculations single and double excitations were allowed from the 6s, 6p, 7s subshells. Natural orbital coefficients were obtained by diagonalizing the averaged density matrices of all components of the $6d^1 7s^2$ 2D valence substate. The generalized contraction scheme was applied to yield (7s6p5d)/[5s4p3d]

ANO valence basis sets. Third, one f function was added and the exponent was optimized for the MRCI energy of the $6d^17s^2$ configuration, yielding the final (7s6p5d1f)/[5s4p3d1f] ANO Gaussian valence basis sets. For the (7s6p5d1f)/[5s4p3d1f] basis sets in the segmented contraction scheme applied here, the contraction coefficients have been taken from the ANO contractions of the lowest energy pseudo-valence orbital in each symmetry in the generalized contracted basis sets. The 5f-in-core PPs and various basis sets of polarized triple to quadruple zeta quality for all actinide elements have been completed for trivalent atoms and will be published in the near future¹⁹.

All other atoms were treated at the AE level. The standard double-zeta (DZ, (8s4p)/[4s2p] for C, N, O and (4s)/[2s] for H) plus polarization (DZP, DZ augmented by a (1d) set for C, N, O or a (1p) set for H) basis sets in TURBOMOLE 20 were used.

The calculations for An-Motex²⁺ were carried out with the TURBOMOLE program package²⁰. The computational method was Becke's semiempirically parameterized gradient-corrected exchange-correlation hybrid density functional approach (B3LYP)^{23, 24, 25}. The geometry of An-Motex²⁺ (Ln=Ac, Cm, Lr) was fully optimized without any symmetry restriction at the DFT/B3LYP level. The electron affinity was calculated by subtracting the energy of An-Motex²⁺ from An-Motex⁺. Similarly, the metal-ligand binding energy was obtained by subtracting the energy of An-Motex²⁺ from the possible dissociation products (Anⁿ⁺, Motex⁽²⁻ⁿ⁾⁺, n=1, 2, 3).

In order to get a systematic comparison with the lanthanide series, Ln-Motex²⁺ (Ln=La, Gd, Lu) were calculated too using the same methods we previously applied to Ln-Tex²⁺ (Ln=La, Gd, Lu)¹⁸. The difference between “Motex” and “Tex” arises from the longer side chains of the “Motex” ligand, cf. figure 1.

Calculations taking into account solvent effects were carried out using COSMO (Conductor-like Screening Model), a kind of dielectric continuum model²⁶. The solute molecule is embedded in a dielectric continuum of permittivity ϵ , with the solute forming a cavity within the dielectric. The electric charges within the cavity in the dielectric medium polarize the dielectric continuum outside of the cavity, i.e., surface charge distribution on the interface (screening charges q). This polarization in turn makes a contribution, called the reaction field, to the electric field within the cavity. The total energy of the system may be written as:

$$E(q) = \frac{1}{2} QCQ + QBq + \frac{1}{2} qAq$$

Here Q and q denote in vector notation the N source charges Q_i and the M surface charges q_j , respectively. A , B and C are Coulomb matrices. The actual screening charge distribution q^* minimizes the total energy. Hence we have

$$\begin{aligned} \frac{\partial E(q)}{\partial q} &= B^T Q^T + Aq = 0 \\ q^* &= -A^{-1} B^T Q^T \end{aligned}$$

In order to take into account the finite permittivity ϵ of real solvents, the screening charges are scaled by a factor $1 - 1.5/(\epsilon+0.5)$. We note that for solvents typically used in the preparation of texaphyrin and motexafin complexes, e.g., water ($\epsilon=80.1$) methanol ($\epsilon=33.0$), the scaling factor has values between 0.95 and 0.98 and the assumption of an infinite permittivity is justified. For the cavity generation the following atomic radii (Å) were used in our calculations: C (2.0), N (1.83), O (1.72), H (1.3), La³⁺ (2.05), Gd³⁺ (1.90), Lu³⁺ (1.80), Ac³⁺ (2.24), Cm³⁺ (1.94) and Lr³⁺ (1.72). The values for the lanthanide and actinide ions were chosen to reproduce in COSMO calculations within 0.1 eV accuracy the experimental (La³⁺ 31.7, Gd³⁺ 34.1, Lu³⁺ 36.1 eV)²⁷ and calculated (Ac³⁺

29.1, Cm³⁺ 33.4, Lr³⁺ 37.8 eV)²⁸ hydration free enthalpies, respectively. For all other parameters the default values implemented in TURBOMOLE were adopted.

Results and Discussion

Before we applied the above described PPs and valence basis sets to An-Motex²⁺, we performed test calculations for An³⁺-H₂O (An = Ac, U, Cm, Es, Lr) as well as Ac-Motex²⁺, by choosing two different core definitions for An, i.e., 5f-in-valence SPP (small-core PP with 60-core-electrons, e.g., 29 valence electrons for Ac) and 5f-in-core LPP (large-core PP with 11-valence-electrons, e.g., 78 core electrons for Ac). The results obtained for small and large basis sets for the actinide(III) monohydrate complexes are listed in table 1. It is seen that even for those elements where the 5f orbitals participate in bonding and the 5f-in-core approximation is least likely to work, e.g. for U, the results are in quite reasonable agreement with those of 5f-in-valence calculations. It should be noted that the 5f-in-core results correspond to an average over all states resulting from a superconfiguration, i.e. all states arising from a given 5f subconfiguration and the valence substate, whereas the 5f-in-valence results refer to the lowest state. For An-Motex²⁺ it was found that the disagreements for calculated bond lengths and bond angles by using LPP and SPP are at most 0.004 Å and 0.3°, cf. table 2. Therefore we conclude that the 11-valence-electrons PPs and corresponding basis sets for An are sufficiently accurate for the study on An-Motex²⁺.

A. Molecular Structures

The most important parameters of the fully optimized structures for An-Motex²⁺ (An=Ac, Cm, Lr) and Ln-Motex²⁺ (Ln=La, Gd, Lu) are listed in table 2. Comparing to

Ln-Motex^{2+} , the calculated An-N bond lengths are on average 0.05 Å longer than the corresponding Ln-N bond lengths for Ln-Motex^{2+} . On the other hand, bond distances and bond angles which exclude the metal are only slightly affected by the substitution of different metal (III) cations, e.g., the change of the average internal angle about C (or N) and its next-adjacent atoms within the ring is at most 1.6°.

In analogy to Ln-Motex^{2+} , for all An-Motex^{2+} it is found that the metal cation is located $\Delta(\text{N}_5)$ above the mean N_5 plane, i.e., 0.77 Å, 0.53 Å and 0.20 Å for Ac, Cm and Lr, respectively. The distance of the actinide element to the mean N_5 plane does reflect the size of the metal cation (III), i.e., the larger the ion, the longer the distance obtained. Comparing to Ln-Motex^{2+} the calculated distance $\Delta(\text{N}_5)$ for An-Motex^{2+} is longer, i.e., $\Delta(\text{N}_5)$ of An-Motex^{2+} for An=Ac, Cm, Lr is 0.04, 0.13, and 0.15 Å larger than of Ln-Motex^{2+} for Ln=La, Gd, Lu, respectively. Therefore the metal ligand bond in An-Motex^{2+} is expected to be weaker than in Ln-Motex^{2+} , mainly due to the larger ion radii of actinide(III) compared to lanthanide(III) ions.

B. Charge Distribution and Frontier Orbitals

The Mulliken orbital populations (cf. table 3) show very similar charge distributions for Ln-Motex^{2+} and An-Motex^{2+} . A relatively constant valence d occupation is observed, i.e., ≈ 0.8 electrons occupation for 6d of all An-Motex^{2+} and ≈ 0.9 electrons occupation for 5d of all Ln-Motex^{2+} , respectively. This indicates covalent metal-ligand bonding contributions from the valence d shell, i.e., substantial deviations from a purely ionic complex between $\text{M}^{3+} [\text{f}^n] \text{s}^2\text{p}^6$ and Motex^{1-} ions. The valence s and p shells get more occupied with the increasing nuclear charge along the lanthanide and actinide series, e.g.,

the 7s/7p occupation increases from 0.20/0.07 for Ac-Motex²⁺ to 0.37/0.26 for Lr-Motex²⁺. We attribute the constant valence d and increasing valence s, p occupations to increasing relativistic effects along the lanthanide and actinide series as well as to shell structure effects due to the filling of the nf (n=4 for Ln and 5 for An) shell, i.e., the f element contraction, cf. table 4. When going from Ac to Lr, the 7s, 7p orbitals contract significantly ($\Delta\langle r \rangle_{7s} = -0.91 \text{ \AA}$, $\Delta\langle r \rangle_{7p} = -0.76 \text{ \AA}$) and get energetically stabilized ($\Delta\epsilon_{7s} = -2.05 \text{ eV}$, $\Delta\epsilon_{7p} = -0.28 \text{ eV}$). The 6d orbital contracts moderately ($\Delta\langle r \rangle_{6d} = -0.45 \text{ \AA}$). It gets energetically stabilized ($\Delta\epsilon_{6d} = -0.46 \text{ eV}$) from Ac to Cm, but becomes less stable ($\Delta\epsilon_{6d} = 0.58 \text{ eV}$) from Cm to Lr. For the lanthanide series the corresponding data for the 6s, 6p and 5d orbitals are: $\Delta\langle r \rangle_{6s} = -0.80 \text{ \AA}$, $\Delta\langle r \rangle_{6p} = -0.72 \text{ \AA}$, $\Delta\epsilon_{6s} = -1.52 \text{ eV}$, $\Delta\epsilon_{6p} = -0.33 \text{ eV}$, $\Delta\langle r \rangle_{5d} = -0.24 \text{ \AA}$, $\Delta\epsilon_{5d} = 0.87 \text{ eV}$, when going from La to Lu, cf. table 4.

Due to their relatively small ionic radii the metal cations are efficiently complexed by the five nitrogen atoms of the macrocyclic skeleton and high metal-ligand binding energies for all lanthanide(III) and actinide(III) motexafins are expected. Whereas the orbital contractions make the cation smaller and allow the formation of nearly planar complexes with higher stability, the orbital stabilization/destabilization clearly favors a charge transfer from the ligand to the metal valence s and p orbitals. As a result an increasing ligand oxidation is found to accompany the insertion of the metal, i.e., the metals carry decreasing positive charges (La-Motex²⁺/Ac-Motex²⁺: 1.67/1.81, Gd-Motex²⁺/Cm-Motex²⁺: 1.66/1.65, Lu-Motex²⁺/Lr-Motex²⁺: 1.60/1.61, cf. table 3).

A quite low LUMO energy is obtained for both lanthanide and actinide complexes, i.e., the LUMO is only $\approx 0.40 \text{ eV}$ and $\approx 0.38 \text{ eV}$ (cf. table 5) higher than the HOMO for Ln-Motex²⁺ and An-Motex²⁺, respectively. Therefore one can expect that both Ln-

Motex²⁺ and An-Motex²⁺ easily absorb electrons in an electron-rich environment, a finding which is supported by experimental evidence in case of the lanthanide systems². It is worthwhile to mention that the energies of the HOMO and LUMO for An-Motex²⁺ are systematically by ≈ 0.02 eV and ≈ 0.10 eV lower than those for Ln-Motex²⁺, respectively.

C. Stability

In order to study the stability of the metal-nitrogen bond in lanthanide(III) and actinide(III) motexfins, the metal-ligand gas phase binding energies are calculated according to three possible dissociation paths ($-E_{\text{bond}} = E(\text{M-Motex}^{2+}) - E(\text{M}^{n+}) - E(\text{Motex}^{(2-n)+})$ with $n=3,2,1$ denoted as paths A, B and C, respectively). In view of the high positive Mulliken charges on the metal (cf. above) only dissociation products with metal cations were considered. The results are summarized in table 5. For all three metal dissociation paths considered the calculated gas phase binding energies for Ln-Motex²⁺ are higher than 10 eV, proving that the Ln-Motex²⁺ complexes are very stable. For An-Motex²⁺ the calculated gas phase binding energies for dissociation paths A, B and C are on average about 1.5, 1.2 and 1.8 eV, respectively, lower compared to Ln-Motex²⁺.

In previous work it was observed that for a fixed valence substate of the lanthanide atoms/ions and compounds as well as a fixed electronic state of the non-lanthanide fragment the binding energy is nearly linear in the lanthanide nuclear charge²⁹. This allows an interpolation of the Ln(An)-Motex²⁺ binding energies for all elements of the 4f(5f) series from the data for La(Ac), Gd(Cm) and Lu(Lr) by linear regression. For Ln-Motex²⁺ the correlation coefficients for paths A, B, and C are 0.9954, 0.9995, and 0.9999, respectively. Correcting from the lanthanide ion state considered in the interpolation to

the experimentally observed Ln^+ and Ln^{2+} ground states with the experimental energy differences yields the typical saw-tooth behavior of the binding energies also observed for other lanthanide compounds²⁹, cf. figure 2. Considering the most favorable dissociation path C in the gas phase we conclude that Gd-Motex^{2+} appears to be the most stable lanthanide(III) motexafin complex, closely followed by Tb-Motex^{2+} . The Eu and Yb compounds should be the least stable systems.

For An-Motex^{2+} the correlation coefficients for paths A, B, and C are 0.9956, 0.9690 and 0.9938, respectively. Unfortunately it is impossible to get binding energies for the whole actinide series by doing corrections from the actinide ion state considered in the interpolation to the experimentally observed ground state with the experimental energy difference, since most of the experimental values for actinide ions are unavailable. Nevertheless, besides the dissociation into $\text{An}^{3+} + \text{Motex}^-$, we still can obtain from the linear regression the gas phase binding energies of two actinide(III) motexafins for dissociation path C where the free actinide ions have the same ground state $5f^n$ subconfiguration ($n=0-14$ for Ac-Lr) as in the complexes as well as the same $7s^2$ valence subconfiguration as Ac^+ , Cm^+ and Lr^+ , i.e., Pa^+ (9.43 eV) and U^+ (9.32 eV). However, considering that the trivalent oxidation state is not preferred for protactinium and uranium, it is suggested to investigate Ac-Motex^{2+} as the best candidate for experimentalists to get stabilization by motexafins.

An alternative way to derive the binding energies with respect to $\text{An}^{2+} + \text{Motex}$ and $\text{An}^+ + \text{Motex}^+$ starts from the results for $\text{An}^{3+} + \text{Motex}^-$ and makes use of the calculated electron affinity (2.83 eV) and ionization potential (5.79 eV) of Motex , as well as estimates of the third and second An ionization potential derived from highly correlated SPP calculations including spin-orbit corrections³⁰. For the cases where the $5f$

subconfiguration does not change the derived values agree well with those obtained from the approach described above, cf. figure 3. A similar procedure can be applied for the lanthanide systems by using corresponding previously published SPP ionization potentials³¹ and also lead to good agreement with the estimates derived by using experimental data (figure 2).

D. Solvent effects

The calculations up to this point considered Ln-Motex²⁺ and An-Motex²⁺ as gas phase species. In order to examine solvent effects on structural and energetic properties we adopted the COSMO, a continuum solvation model. The structures of all Ln-Motex²⁺ and An-Motex²⁺ considered here were reoptimized by taking into account a solvent of infinite permittivity, i.e., the results should be close to those for aqueous solvation. It was found that the geometries of the macrocyclic skeleton are only slightly affected by the solvent, whereas the metal-nitrogen bond lengths are lengthened and $\Delta(N_5)$ is brought into close agreement with the experimental values for Ln-Motex²⁺, cf. table 6. For all complexes the metal-nitrogen bonds involving pyrrole nitrogen are on average increased by 0.05 Å. The amplitude of the change for the metal-nitrogen bonds involving pyrrole nitrogen caused by solvent effects does reflect the size of the metal cation, i.e., the larger the ion, the larger bond length extension obtained, e.g. for actinium(III) and lutetium(III) the metal-nitrogen bonds involving pyrrole nitrogen are on average increased by 0.06 Å and 0.03 Å, respectively. The solvent effects on the metal-nitrogen bonds involving imine nitrogen are slightly smaller, e.g., for Ac-Motex²⁺ the Ac-N bond lengths are increased by 0.06 Å and 0.04 Å for bonds involving pyrrole nitrogen and imine nitrogen, respectively.

Dissociation pathway A most likely would be preferred in aqueous solution and the calculated binding energies for Ln-Motex²⁺ (La 32.05, Gd 34.70, Lu 36.56 eV) are almost as large as the experimentally observed Ln³⁺ hydration energies (La 31.7, Gd 34.1, Lu 36.1 eV)²⁷ in agreement with the existence of water-soluble stable lanthanide motexafin complexes⁵. Although for An-Motex²⁺ the experimental An³⁺ hydration energies are still unavailable, the calculated binding energies (Ac 30.24, Cm 33.28, Lr 35.47 eV) are very similar to the recently calculated An³⁺ hydration energies (Ac 29.1, Cm 33.4, Lr 37.8 eV)²⁸, implying that actinide motexafin complexes might be stable in water too. Under the assumption of nearly equal hydration energies of the Ln-Motex²⁺ and An-Motex²⁺ complexes, these numbers even imply that Ac-Motex²⁺ is the most stable of the six complexes in water. The COSMO results yield stabilities of Ln(An)-Motex²⁺ with respect to Ln(An)³⁺ and Motex⁻ of 3.91(4.81), 4.09(3.94) and 4.15(2.12) eV for La(Ac), Gd(Cm) and Lu(Lr), respectively, and support this view. It is noteworthy that the stabilities of the three Ln-Motex²⁺ systems are almost equal, whereas a clear decrease of the stability is observed for An-Motex²⁺ along the An series.

The electron affinity is an important chemical property related to the LUMO, and high electron affinities were obtained for Ln-Motex²⁺ and An-Motex²⁺ without taking into account solvent effects, i.e., La(Ac)-Motex²⁺: 7.59(7.64) eV, Gd(Cm)-Motex²⁺: 7.61(7.70) eV, Lu(Lr)-Motex²⁺: 7.69(7.72) eV. The main contributions for the LUMO are from atomic orbitals of the main group elements, i.e., N1, N3, N5, C7, C9, C11, C16, C18, C20, C22, and C23. Therefore the added electron is most likely going to the ligand rather than the metal, thus explaining the nearly metal-independent electron affinity. The solvent corrections preferentially stabilize the doubly charged Ln(An)-Motex²⁺ relative to the singly charged ones as expected. As a result, there is a net decrease by about 3.6 eV

in the absolute magnitudes of the electron affinity in solution but the relative order remains unchanged (table 5). The calculated high electron affinity agrees with the conclusion obtained from in vitro experiments which have also proven that Ln-Tex²⁺ is very easily and quasi-reversibly reduced to Ln-Tex⁺ ($E_{1/2} \approx -0.27$ V vs. Ag/AgCl) and Ln-Tex ($E_{1/2} \approx -0.75$ V vs. Ag/AgCl) ³².

Finally we want to note that the results presented in this section depend noticeably on the choice of the effective radii used in the COSMO model. Our choice was based on experimental and theoretical values for the solvation energies of the Ln³⁺/An³⁺ ions adopted from consistent data for free enthalpies of hydration stemming from similar sources. Different choices of these radii within reasonable limits lead to qualitatively similar results, e.g., Ac-Motex²⁺ is most stable, provided that they reflect the lanthanide/actinide contractions and the fact, that the An³⁺ ions are slightly larger than the Ln³⁺ ions. We feel that correctly modeling the solvation for the systems studied here is a much more critical point than the approximation of putting the 5f shell into the PP core. However, developing better models of solvation, e.g., by treating the water molecules in the first coordination sphere explicitly, is beyond the scope of the present work and clearly a task for the future.

Conclusions

The molecular structures and chemical/physical properties (stability, electron affinity) of actinide(III) motexafins (An-Motex²⁺, An=Ac, Cm, Lr) were calculated using a DFT/B3LYP method in connection with scalar-relativistic energy-consistent 5f-in-core actinide pseudopotentials. The results have been discussed with a comparison to Ln-Motex²⁺ (Ln=La, Gd, Lu). In analogy to Ln-Motex²⁺ the structures of An-Motex²⁺ do

reflect the cation employed, i.e., the larger the cation, the greater the out-of plane displacement $\Delta(N_5)$ of the metal from the mean N_5 plane. $\Delta(N_5)$ for An-Motex²⁺ (An=Ac, Cm, Lr) is 0.02, 0.09, and 0.15 Å larger than for Ln-Motex²⁺ (Ln=La, Gd, Lu), respectively. Although both lanthanide(III) and actinide(III) motexafins have quite high gas phase binding energies with respect to the three dissociations paths $M^{3+} + \text{Motex}^-$, $M^{2+} + \text{Motex}$ and $M^+ + \text{Motex}^+$, the calculated values for the actinide systems are on average about 1.3, 1.0 and 1.8 eV, respectively, smaller than for the lanthanide complexes. The actinium (III) motexafin has been concluded to be the most stable actinide(III) motexafin in gas phase. It was found that both Ln-Motex²⁺ (Ln=La, Gd, Lu) and An-Motex²⁺ (An=Ac, Cm, Lr) have a relatively low LUMO located mainly on the macrocycle, i.e., the LUMO is only about 0.39 eV higher than the HOMO, resulting in a high, nearly metal-independent electron affinity of ≈ 7.6 eV.

The geometries of the macrocyclic skeletons of Ln-Motex²⁺ and An-Motex²⁺ are only slightly affected by a solvent with infinite permittivity taken into account by the conductor-like screening model, whereas the position of the complexed cation changes significantly, e.g., the $\Delta(N_5)$ values of Ln-Motex²⁺ are brought into close agreement with experimental data. In addition, the solvent corrections result in a net decrease of about 3.5 eV in the absolute magnitudes of the electron affinity in solution, whereas the relative order remains unchanged. Ac-Motex²⁺ is found to be the most stable complex and should be the best candidate for experimentalists to get stabilization of An³⁺ by motexafin.

Acknowledgments

The authors are grateful to Prof. J. L. Sessler for bringing the topic of actinide motexafin complexes to their attention. The financial support of CSC (China Scholarship

Council) and DAAD (German Academic Exchange Service) is gratefully acknowledged.

Tables

Table 1 Bond lengths (\AA) and binding energies (eV) for $M\text{-H}_2\text{O}^{3+}$ ($M=\text{Ac, U, Cm, Es, Lr}$) complexes from 5f-in-core large-core (LC) and 5f-in-valence small-core (SC) PP HF calculations using small/large basis sets.*

	R_e		D_e	
	PP LC	PP SC	PP LC	PP SC
Ac	2.47/2.45	2.47/2.45	3.55/3.25	3.55/3.33
U	2.39/2.38	2.36/2.35	3.83/3.53	3.94/3.73
Cm	2.31/2.30	2.30/2.28	4.16/3.87	4.22/4.01
Es	2.26/2.25	2.24/2.23	4.39/4.10	4.46/4.27
Lr	2.19/2.19	2.20/2.19	4.69/4.40	4.70/4.51

* basis sets: small basis sets: PP LC (8s7p6d2f); PP SC (14s13p10d8f)/[6s6p5d4f]; H, O cc-pVDZ; large basis sets: PP LC (8s7p6d2f1g); PP SC (14s13p10d8f6g)/[6s6p5d4f3g]; H, O aug-cc-pVQZ.

Table 2 Selected bond lengths (Å) and angles (deg) for M-Motex²⁺ (M=La, Gd, Lu, Ac, Cm, Lr) calculated at the B3LYP level. *

	La	Ac	Ac(SPP*)	Gd	Cm	Lu	Lr
N3	2.529	2.588	2.585	2.440	2.486	2.387	2.403
N2	2.434	2.501	2.499	2.342	2.396	2.283	2.321
N4	2.433	2.500	2.499	2.342	2.396	2.283	2.321
N5	2.613	2.682	2.685	2.516	2.571	2.463	2.490
N1	2.615	2.682	2.685	2.516	2.571	2.457	2.490
$\Delta(N_5)^a$	0.75	0.77	0.78	0.40	0.53	0.05	0.20
C16,C11 ^b	129.3	130.1	129.9	129.0	129.5	128.3	129.1
C21,C6 ^b	118.8	119.0	119.0	118.6	118.7	118.1	118.5
N5,N1 ^b	124.6	124.8	124.7	124.3	124.4	123.4	124.1
Np ^c	74.6	73.1	73.0	77.4	75.8	78.6	78.2
Np,i ^c	63.5	63.7	63.6	67.9	66.4	69.1	68.5
Ni ^c	61.5	60.1	59.8	63.9	62.5	64.7	64.5

* Unless otherwise noted, the distance (Å) given is for the separation between the indicated atom and the lanthanide/actinide(III) cation. 46/78-, 53/85-, 60/92-electron core PPs were applied for La/Ac, Gd/Cm, Lu/Lr, respectively. SPP: 60-electron core PP for Ac. Standard (7s6p5d)/[5s4p3d] valence basis sets augmented by (1s1f) sets and (7s6p5d1f)/[5s4p3d1f] valence basis sets used for lanthanides and actinides, respectively. DZP basis sets for C, H, O, N.

a The distance (Å) to the lanthanide/actinide(III) cation from the average plane through the five nitrogen atoms.

b Refers to the average internal angle about this atom and its next-adjacent atom within the ring; i.e., C16,C11 denotes the average angle about these two mesolike methine carbons, namely C17-C16-C15 and C12-C11-C10, respectively.

c Np refers to the average N-Metal-N angle involving adjacent pyrrole nitrogens, i.e., N3-Metal-N4; Np,i refers to the average N-Metal-N angle involving a pyrrole nitrogen and that of its adjacent imine; Ni is the N-Metal-N angle defined by the two imine nitrogens.

Table 3 Mulliken orbital populations and atomic charges (Q) on M (metal) (M=La, Gd, Lu, Ac, Cm, and Lr) and nitrogens in lanthanide(III)/actinide(III) motexafins .

	s	p	d	f	Q
La/Ac	2.17/2.20	6.11/6.07	1.01/0.87	0.04/0.04	1.67/1.81
N3	3.67/3.64	3.92/3.97	0.02/0.03	-	-0.61/-0.64
N2	3.65/3.64	3.95/3.97	0.03/0.03	-	-0.62/-0.64
N1	3.62/3.61	3.84/3.85	0.03/0.03	-	-0.48/-0.49
N5	3.62/3.61	3.84/3.85	0.03/0.03	-	-0.48/-0.49
N4	3.65/3.66	3.94/3.95	0.03/0.02	-	-0.62/-0.63
Gd/Cm	2.21/2.28	6.21/6.18	0.90/0.87	0.01/0.01	1.66/1.65
N3	3.67/3.64	3.94/3.97	0.02/0.02	-	-0.64/-0.64
N2	3.65/3.64	3.97/3.97	0.02/0.02	-	-0.65/-0.64
N1	3.62/3.62	3.86/3.85	0.02/0.03	-	-0.50/-0.49
N5	3.61/3.62	3.89/3.85	0.03/0.03	-	-0.52/-0.49
N4	3.65/3.66	3.97/3.94	0.02/0.02	-	-0.65/-0.62
Lu/Lr	2.29/2.37	6.31/6.26	0.80/0.75	0.00/0.01	1.60/1.61
N3	3.67/3.64	3.94/3.98	0.02/0.02	-	-0.63/-0.64
N2	3.65/3.64	3.98/3.98	0.02/0.02	-	-0.65/-0.64
N1	3.62/3.62	3.98/3.85	0.02/0.03	-	-0.50/-0.50
N5	3.62/3.62	3.85/3.85	0.03/0.03	-	-0.50/-0.50
N4	3.65/3.66	3.98/3.94	0.02/0.02	-	-0.65/-0.63

A $5s^2 5p^6 5d^1 6s^2$ and $6s^2 6p^6 6d^1 7s^2$ ground-state valence subconfigurations are considered for the lanthanide and actinide elements, respectively; 0, 7 and 14 electrons in the 4f/5f shell are attributed to the PP core for La/Ac, Gd/Cm, Lu/Lr, respectively.

Table 4 $\langle r \rangle$ -expectation values (a.u.) and negative orbitals energies $-\epsilon$ (a.u.) for the 5d, 6s, and 6p orbitals of Ln in their $4f^n 5d^1 6s^1 6p^1$ configurations, 6d, 7s and 7p orbitals of An in their $5f^n 6d^1 7s^1 7p^1$ configurations from scalar-relativistic (WB) all-electron calculations.

Metal	$\langle r \rangle_{5d}/\langle r \rangle_{6d}$	$\langle r \rangle_{6s}/\langle r \rangle_{7s}$	$\langle r \rangle_{6p}/\langle r \rangle_{7p}$	$-\epsilon_{5d}/-\epsilon_{6d}$	$-\epsilon_{6s}/-\epsilon_{7s}$	$-\epsilon_{6p}/-\epsilon_{7p}$
La/Ac	2.819/3.327	4.547/4.435	6.207/6.512	0.271/0.218	0.223/0.239	0.118/0.112
Gd/Cm	2.615/2.930	4.106/3.917	5.797/6.049	0.266/0.235	0.250/0.275	0.125/0.118
Lu/Lr	2.579/2.875	3.747/3.525	5.485/5.755	0.239/0.213	0.279/0.314	0.130/0.123

Table 5 Calculated M-Motex²⁺ (M=La, Gd, Lu, Ac, Cm, Lr) bond energies (E_{bond}), electron affinities (EA), HOMO and LUMO energies, all in units of eV. The bond energies for dissociation path A as well as the electron affinities corrected for effects of a solvent of infinite permittivity are listed in the second row (solv.).

	La/Ac	Gd/Cm	Lu/Lr
$E_{\text{bond}}^{\text{a}}$	32.10/30.24	34.70/33.28	36.56/35.47
solv.	3.91/4.81	4.09/3.94	4.15/2.12
$E_{\text{bond}}^{\text{b}}$	15.82/15.51	17.50/16.31	18.59(19.00)/16.62
$E_{\text{bond}}^{\text{c}}$	10.29/9.60	11.20(12.00)/8.97	10.56(13.70)/8.04
EA	7.59/7.64	7.61/7.70	7.69/7.72
solv.	3.99/4.00	4.01/3.96	3.96/3.97
$-E_{\text{HOMO}}$	8.91/9.01	8.91/9.01	9.00/9.03
$-E_{\text{LUMO}}$	8.52/8.59	8.53/8.65	8.56/8.67

^a $-E_{\text{bond}}=E(\text{M-Motex}^{2+})-E(\text{M}^{3+})-E(\text{Motex}^{\cdot-})$; the ground state configurations are $d^0 \ ^1S_0$ for La^{3+} and Ac^{3+} , $f^7d^0 \ ^8S_{7/2}$ for Gd^{3+} and Cm^{3+} , $f^{14}d^0 \ ^1S_0$ for Lu^{3+} and Lr^{3+} , respectively.

^b $-E_{\text{bond}}=E(\text{M-Motex}^{2+})-E(\text{M}^{2+})-E(\text{Motex}^{\cdot-})$; the configurations are $d^1 \ ^2D_{3/2}$ for La^{2+} and $s^1 \ ^2S_{1/2}$ for Ac^{2+} , $f^7d^1 \ ^9D_2$ for Gd^{2+} and $f^7s^1 \ ^9S_4$ for Cm^{2+} , $f^{14}s^1 \ ^2S_{1/2}(f^{14}d^1 \ ^2D_{3/2})$ for Lu^{2+} and $f^{14}s^1 \ ^2S_{1/2}$ for Lr^{2+} , respectively.

^c $-E_{\text{bond}}=E(\text{M-Motex}^{2+})-E(\text{M}^+)-E(\text{Motex}^{\cdot+})$; the configurations are $d^2 \ ^3F_2$ for La^+ and $s^2 \ ^1S_0$ for Ac^+ , $f^7d^1s^1 \ ^{10}D_{5/2}(f^7d^2 \ ^{10}F_{3/2})$ for Gd^+ and $f^7s^2 \ ^8S_{7/2}$ for Cm^+ , $f^{14}s^2(f^{14}d^2 \ ^3F_2) \ ^1S_0$ for Lu^+ and $f^{14}s^2 \ ^1S_0$ for Lr^+ , respectively.

Table 6 Selected bond lengths (Å) and angles (deg) for M-Motex²⁺ (M=La, Gd, Lu, Ac, Cm, Lr) calculated at the B3LYP level with the inclusion of solvent effects by using COSMO. For other explanations cf. table 2.

	La	Ac	Gd	Cm	Lu	Lr
N3	2.607	2.657	2.500	2.539	2.426	2.473
N2	2.500	2.558	2.385	2.431	2.312	2.367
N4	2.500	2.558	2.385	2.431	2.313	2.367
N5	2.654	2.720	2.540	2.591	2.464	2.522
N1	2.659	2.720	2.544	2.591	2.466	2.522
$\Delta(N_5)^a$	0.92	0.97	0.61	0.64	0.15	0.41
(exp.)	(0.91)		(0.58)		(0.27)	
C16,C11 ^b	129.6	123.0	129.2	129.6	129.0	129.5
C21,C6 ^b	118.5	118.6	118.2	118.4	118.0	118.3
N5,N1 ^b	125.0	124.9	124.6	124.5	124.1	124.4
Np ^c	72.5	70.9	75.8	74.4	78.4	76.6
Np,i ^c	63.8	62.3	66.8	65.5	68.7	67.3
Ni ^c	60.7	59.1	63.4	62.0	65.4	63.9

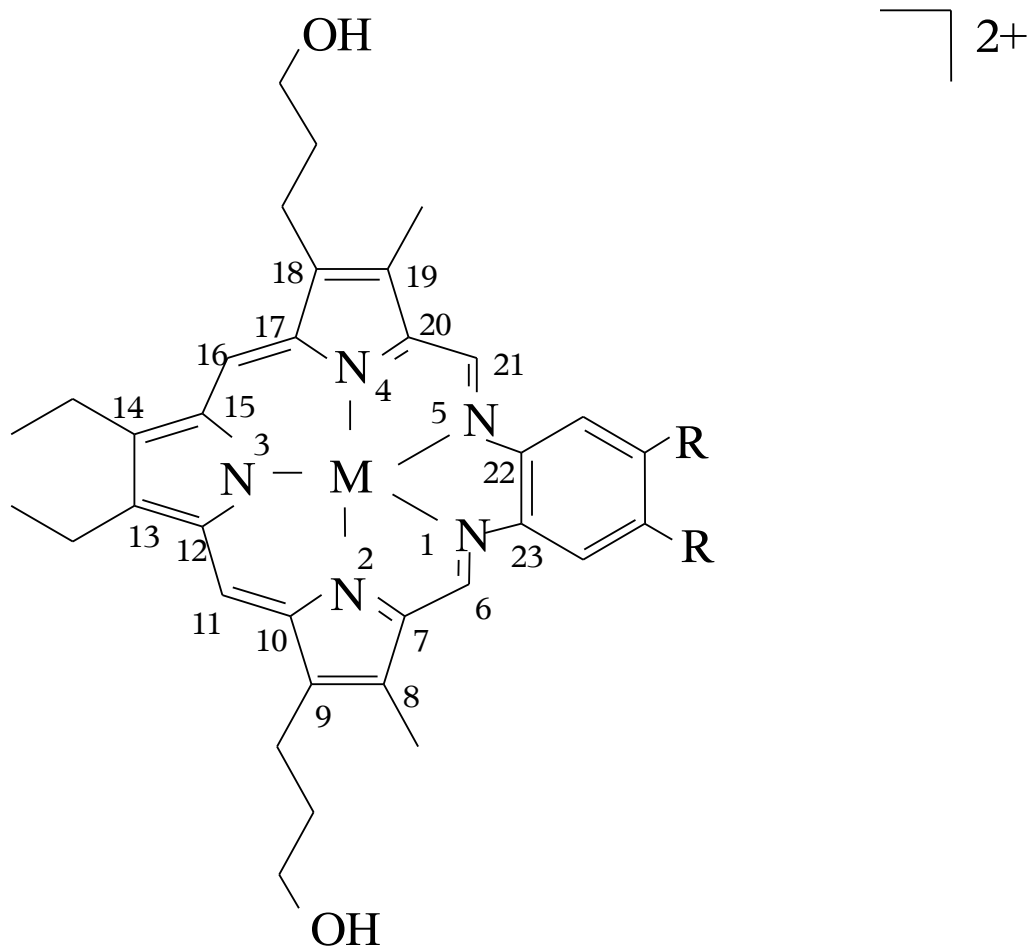
Figure captions

Fig. 1 Structures for lanthanide(III) and actinide(III) texaphyrins ($M\text{-Tex}^{2+}$) and motexafins ($M\text{-Motex}^{2+}$), $M = \text{La, Gd, Lu, Ac, Cm, Lr}$.

Fig. 2 Ln-Motex^{2+} binding energies for three dissociation channels (A: $\text{Ln}^{3+} + \text{Motex}^-$, B: $\text{Ln}^{2+} + \text{Motex}$, C: $\text{Ln}^+ + \text{Motex}^+$) for all lanthanide elements from the calculated data for La, Gd, and Lu by linear regression and interpolation (stars). The lanthanide ions are assumed to have $\text{Ln}^{3+} 4f^n$, $\text{Ln}^{2+} 4f^n 5d^1$ and $\text{Ln}^+ 4f^n 5d^2$ configurations, i.e., the same 4f subconfiguration as in the complex. For channel A the values correspond to the complex binding energies. For channels B and C binding energies obtained after experimentally and theoretically obtained corrections to the actual ground states of Ln^{2+} and Ln^+ (cf. text) are denoted by filled and empty symbols, respectively.

Fig. 3 As figure 2, but for An-Motex^{2+} based on data for Ac, Cm, and Lr. The actinide ion configurations used in the linear regression and interpolation are $\text{An}^+ 5f^n$, $\text{An}^{2+} 5f^n 7s^1$ and $\text{An}^+ 5f^n 7s^2$.

Figure 1



$M = \text{La, Gd, Lu; Ac, Cm, Lr}$

a) $R = \text{O}(\text{CH}_2)_3\text{OH}$, texaphyrin

b) $R = \text{O}(\text{CH}_2\text{CH}_2\text{O})_3\text{CH}_3$, motexafin

Figure 2

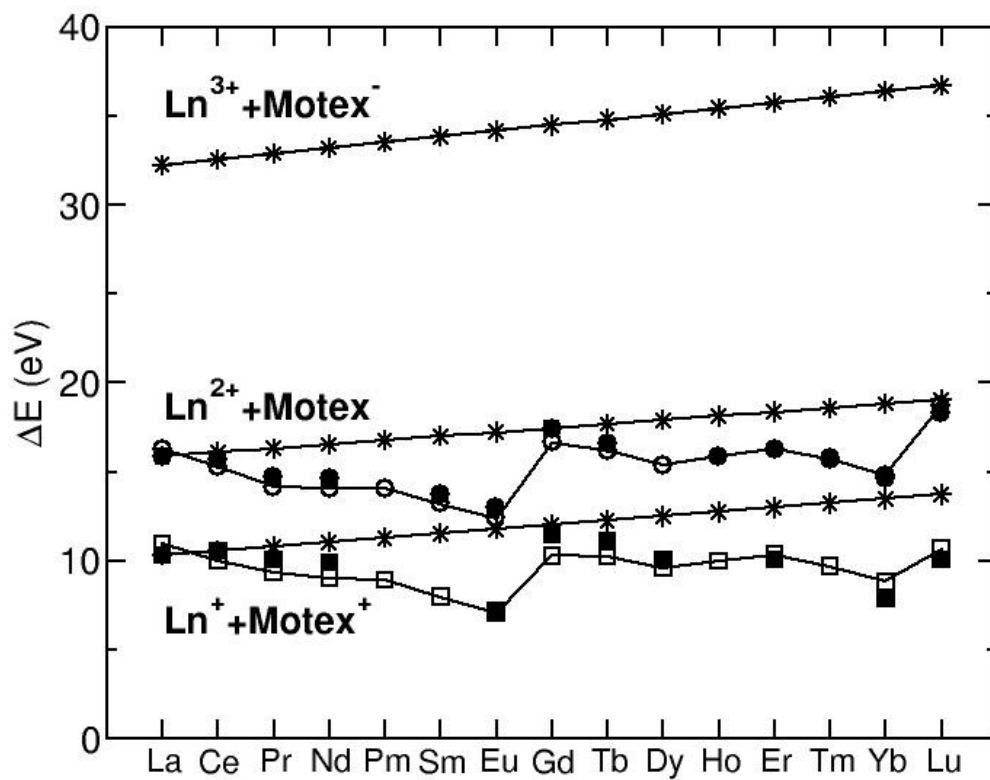
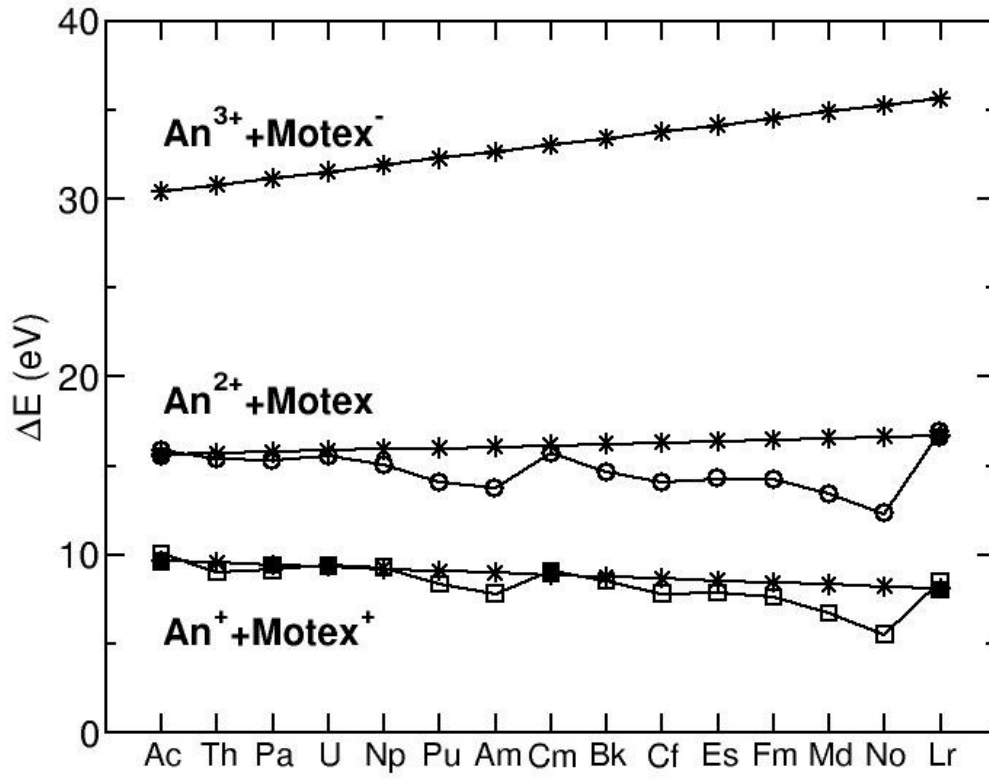


Figure 3



References

- ¹ Sessler, J. L.; Murai, T.; Lynch, V.; Cyr, M. J. *Am. Chem. Soc.* 1988, 110, 5586-5588.
- ² Mody, T. D.; Fu, L.; Sessler, J. L., In *Progress in Inorganic Chemistry*; Karlin K.D., Ed.; John Wiley & Sons, Inc: New York, 2001; Vol. 49: 551-598.
- ³ Mody, T. D.; Sessler, J. L. In *Supramolecular Materials and Technologies*; Reinhoudt, D. N., Ed.; Wiley: Chichester, 1999; Vol. 4: p.245-294.
- ⁴ Sessler, J. L.; Hemmi, G.; Mody, T. D.; Murai, T.; Burrell, A.; Young, S.W. *Acc. Chem. Res.* 1994, 27, 43-50.
- ⁵ Sessler, J. L.; Mody, T. D.; Hemmi, G. M.; Vincent, L., *Inorg. Chem.* 1993, 32, 3175-3187.
- ⁶ Young, S. W.; Qing, F.; Harriman, A.; Sessler, J. L.; Dow, W. C.; Mody, T. D.; Hemmi, G. W.; Hao, Y. P.; Miller, R. A. *Proc. Natl. Acad. Sci. USA* 1996, 93, 6610-6615.
- ⁷ Rosenthal, D. I.; Nurenberg, P.; Becerra, C. R.; Frenkel, E. P.; Carbone, D. P.; Lum, B. L., Miller, R.; Engel, J.; Young, S.; Miles, D.; Renschler, M. F. *Clin. Cancer Res.* 1999, 5, 739-745.
- ⁸ Rockson, S. G.; Kramer, P.; Razavi, M.; Szuba, A.; Filardo, S.; Adelman, D. C. *Circulation* 2000, 102, 2322-2324.
- ⁹ Sessler, J. L.; Vivian, A. E.; Seidel, D.; Burrell, A. K.; Hoehner, M.; Mody, T. D.; Gebauer, A.; Weghorn, S. J.; Lynch, V. *Coord. Chem. Rev.* 2001, 216-217, 411-434.
- ¹⁰ Kimura, H.; Takano, H.; Muromura, T. *J. Nucl. Mater.* 1999, 274, 197-205.
- ¹¹ Dolg, M. In *Encyclopedia of Computational Chemistry*; Schleyer, P. v. R.; Allinger, N. L.; Clark, T.; Gasteiger, J.; Kollman, P. A.; Schaefer III H. F.; Schreiner P. R., Eds.; Wiley: Chichester, 1998; pp 1478-1486.
- ¹² Kutzelnigg, W. *Phys. Scr.* 1987, 36, 416.
- ¹³ Dolg, M.; Stoll, H.; Savin, A.; Preuss, H. *Theor. Chim. Acta* 1989, 75, 173-194.
- ¹⁴ Dolg, M.; Stoll, H.; Preuss, H. *J. Chem. Phys.* 1989, 90, 1730-1734.
- ¹⁵ Cao, X.; Dolg, M. *J. Chem. Phys.* 2001, 115, 7348-7355.
- ¹⁶ Küchle, W.; Dolg, M.; Stoll, H.; Preuss, H. *J. Chem. Phys.* 1994, 100, 7535-7542.
- ¹⁷ Cao, X.; Dolg, M. *J. Chem. Phys.* 2003, 118, 487-496.
- ¹⁸ Cao, X.; Dolg, M. *Mol. Phys.* 2003, 101, 2427-2435.
- ¹⁹ Moritz, A.; Cao, X.; Dolg, M. to be published.
- ²⁰ TURBOMOLE is a program package developed by the Quantum Chemistry Group at the University of Karlsruhe, Germany, since 1988. Ahlrichs, R.; Bär, M.; Häser, M.; Horn, H.; Kölmel, C. *Chem. Phys. Lett.* 1989, 162, 165-169.
- ²¹ Dolg, M.; Stoll, H.; Preuss, H. *Theor. Chim. Acta* 1993, 85, 441-450.
- ²² Dolg, M.; Wedig, U.; Stoll, H.; Preuss, H. *J. Chem. Phys.* 1987, 86, 866-872.

- ²³ Becke, A. D. J. Chem. Phys. 1993, 98, 5648-5652.
- ²⁴ Lee, C.; Yang, W.; Parr, R. G. Phys. Rev. B 1988, 37, 785-789.
- ²⁵ Stephens, P. L.; Devlin, F. J.; Chabalowski, C.F.; Frisch, M. J. J. Phys. Chem. 1994, 98, 11623-11627.
- ²⁶ Klamt, A.; Schuurmann, G. J. Chem. Soc. Perkin Trans. 1993, 2, 799-805.
- ²⁷ David, F.; Vokhmin, V., Ionova, G. J. Mol. Liq. 2001, 90, 45-62.
- ²⁸ David, F. H.; Vokhmin, V. New J. Chem. 2003, 27, 1627-1632.
- ²⁹ Dolg, M.; Stoll, H. Electronic structure calculations for molecules containing lanthanide atoms; In Handbook on the Physics and Chemistry of Rare Earths; Gschneidner Jr., K. A.; Eyring L., Eds. Elsevier: Amsterdam, 1996:
- ³⁰ Cao, X.; Dolg, M. Mol. Phys. 2003, 101, 961-969.
- ³¹ Cao, X.; Dolg, M. Chem. Phys. Lett. 2001, 115, 7348-7355.
- ³² Sessler, J. L.; Tvermoe, N. A.; Guldi, D. M.; Mody, T. D.; Allen, W. E. J. Phys. Chem. A 1999, 103, 787-794.

Synopsis

Density functional studies of actinide (III) motexafins (An-Motex²⁺, An = Ac, Cm, Lr). Structure, stability and comparison with lanthanide (III) motexafins

Xiaoyan Cao, Quansong Li, Anna Moritz, Zhizhong Xie, Michael Dolg, Xuebo Chen, Weihai Fang

Quantum chemical first-principles calculations predict actinide(III) complexes of the motexafin macrocycle to have a similar stability as the corresponding lanthanide systems. The actinium(III) motexafin complex is even predicted to have the highest stability of all 4f- and 5f-element systems in aqueous solution.

